



NIH Public Access

Author Manuscript

Biomacromolecules. Author manuscript; available in PMC 2013 November 03.

Published in final edited form as:

Biomacromolecules. 2008 August ; 9(8): . doi:10.1021/bm800113g.

New Design of Helix Bundle Peptide–Polymer Conjugates

Jessica Y. Shu[†], Cen Tan[†], William F. DeGrado[‡], and Ting Xu^{*,†,§,||}

[†]Department of Materials Science and Engineering, University of California, Berkeley, California 94720

[‡]Department of Biochemistry and Biophysics, School of Medicine, University of Pennsylvania, Philadelphia, Pennsylvania 19104

[§]Department of Chemistry, University of California, Berkeley, California 94720

^{||}Materials Sciences Division, Lawrence Berkeley National Laboratory, Berkeley, California 94720

Abstract

We present a new design of peptide–polymer conjugates where a polymer chain is covalently linked to the side chain of a helix bundle-forming peptide. The effect of conjugated polymer chains on the peptide structure was examined using a de novo designed three-helix bundle and a photoactive four-helix bundle. Upon attachment of poly(ethylene glycol) to the exterior of the coiled-coil helix bundle, the peptide secondary structure was stabilized and the tertiary structure, that is, the coiled-coil helix bundle, was retained. When a heme-binding peptide as an example is used, the new peptide–polymer conjugate architecture also preserves the built-in functionalities within the interior of the helix bundle. It is expected that the conjugated polymer chains act to mediate the interactions between the helix bundle and its external environment. Thus, this new peptide–polymer conjugate design strategy may open new avenues to macroscopically assemble the helix bundles and may enable them to function in nonbiological environments.

Introduction

Peptide-polymer conjugates have the potential to combine the advantages of synthetic polymers, peptides, and peptidomimetics and can lead to hierarchically ordered, functional soft materials.^{1–12} Various types of peptide–polymer conjugates have been designed and investigated. Most are linear di- or triblock copolymers and can be divided into two families based on the complexity of the peptide sequences and the specificity of the intra- and interpeptide interactions. The first family consists of an amino acid homopolymer as one block and either a synthetic polymer or polypeptide as the second block. The peptide homopolymer typically forms secondary structures and, upon phase separation of the block copolymer, assembles within microdomains, resulting in hierarchical assemblies with subnanometer features.^{6,10,11} Although specific interactions, such as electrostatic interactions and hydrogen bonding, have been introduced between each block to direct and manipulate the conjugate assemblies, the peptide’s built-in functionalities associated with a unique sequence are lost. The second family of peptide–polymer conjugates contains a specific peptide sequence with tailored intra- and interpeptide interactions. Peptides forming α -helices and β -sheets, as well as cyclic peptides, have been used as building

© 2008 American Chemical Society

*To whom correspondence should be addressed. tingxu@berkeley.edu.

Supporting Information Available. MALDI-TOF spectra of all the peptide–PEG conjugates and detailed information on the heme titration experiments and data analysis. This material is available free of charge via the Internet at <http://pubs.acs.org>.

blocks.^{1,4,5,7–9,13–19} With these, hierarchical assemblies having molecular level control over chemical heterogeneity have been achieved. Furthermore, peptides forming tertiary structures, such as the leucine zipper, have also been used as physical cross-linking points to generate hydrogels for tissue engineering.^{7,8,20} There have been, however, limited studies on peptide–polymer conjugates that utilize the built-in functionalities of helix bundles to achieve high selectivity, specificity or responsiveness to external stimuli, as observed in natural proteins.

Coiled-coil helix bundles, found in more than 200 natural proteins, underpin many structural and catalytic functions of natural proteins, such as enzymatic activity, signal transfer and redox chemistry. Recently, a large number of peptide sequences forming helix bundles have been de novo designed (designed with novel amino acid sequences) to not only mimic natural protein functionalities, but also to perform functions not seen in nature.^{21–30} These peptides have both chemical and structural diversity that are comparable to or greater than those found in natural materials and are typically more robust.³¹ They are, however, limited by stability and degradation encountered during handling and are not amenable to standard fabrication processes that generate technologically important functional materials. Upon conjugating synthetic polymers to the helix bundle and obtaining proper assemblies, the synthetic polymers could act to protect, deliver and template the peptides on the nanometer scale, while the peptide bundles could provide molecular level control over the chemical heterogeneity to trigger, direct, and execute built-in functionalities.^{1,3,32} The success in achieving desirable, functional assemblies relies on fundamentally understanding the interactions between each building block and delicately balancing and manipulating these interactions to achieve targeted assemblies without interfering with helix bundle formation or designed functionalities.

We have designed and studied a new family of helix bundle-forming peptide–polymer conjugates, with the polymer chain covalently linked to the peptide side chain. Upon attaching poly(ethylene glycol) (PEG) chains to the exterior of a previously de novo designed three-helix bundle, the peptide secondary structure is stabilized. Also, the presence of PEG does not interfere with the peptide tertiary structure, that is, the coiled-coil helix bundle. More importantly, using a photoactive, heme-binding, four-helix bundle-forming peptide as an example, this new design preserves the built-in functionalities within the interior of the helix bundle. This design strategy for peptide–polymer conjugates opens a new avenue toward generating functional biomaterials that use more sophisticated peptide structures to achieve high selectivity, sensitivity and responsiveness, as seen in nature. With the unique architecture of this designed peptide–polymer conjugate, the peptide structure is retained and both termini of the peptide are accessible, making it feasible to generate hydrogels with tailored spatial distributions and aggregation states of chemical motifs for tissue engineering. More importantly, the polymer chains on the exterior of the helix bundle could provide a handle to mediate interactions with the external environment, could potentially enable the macroscopic self-assembly of the helix bundles, and could allow the helix bundle-based machineries to function in nonbiological environments. With the chemical and structural diversity of either naturally existing or de novo designed helix bundles and the many advantages of synthetic polymers, the prospect of fabricating materials with novel properties, superior to natural materials, is clearly possible.

Materials and Methods

Materials

Two peptides, referred hereafter as 1CW (Ac-EVEALE-KKVAALESKVQALEKKVEALEHG WDGR-CONH₂) and H10H24 (Ac-GGGEIWKLHEEFLKKFEELLKLHEERLKKM-CONH₂) were investigated.^{33,34} The

peptides were synthesized on an AAPTEC Apex 396 solid phase synthesizer using standard 9-fluorenylmethyl carbamate (Fmoc) protection chemistry on Wang resin (Nova Biochem), typically at 0.3 mmol scale. The side chain protecting groups were as follows: Lys(Boc), Glu(OtBu), Asp(OtBu), Cys(Trt), Arg(Pbf), His(Trt), Trp-(Boc), Ser(tBu), Gln(Trt). For the synthesis of 1CW-PEG conjugates, the serine at position 14 was mutated to cysteine to facilitate conjugation of maleimide end-functionalized PEG. Similarly for H10H24, the lysine at position 15 was mutated to cysteine. Prior to peptide cleavage from the resin, the N-terminus was acetylated using a 1:1 (v/v) acetic anhydride: pyridine solution for 30 min. The peptides were cleaved from the resin and simultaneously deprotected using 90:8:2 trifluoroacetic acid (TFA)/ethanediol/water for 3.5 h. Crude peptides were precipitated in cold ether and subsequently dissolved in water and lyophilized. Maleimide end-functionalized PEG, purchased from Rapp Polymere (Germany), was then coupled to the cysteine residues of the peptides, which were in white powder form, in 25 mM potassium phosphate buffer at pH 8 for 1 h.³ PEGs of three varying molecular weights were utilized: 750, 2000, and 5000 Da. These are referred henceforth as PEG750, PEG2K, and PEG5K, respectively.

Reversed-Phase High-Pressure Liquid Chromatography (RPHPLC)

Peptides and their conjugates were purified by RP-HPLC (Beckman Coulter) on a C18 column (Vydac). Samples were eluted with a linear AB gradient, where solvent A consisted of water plus 0.1% (v/v) TFA and solvent B consisted of acetonitrile plus 0.1% (v/v) TFA. For purification of 1CW and its conjugates, the linear AB gradient of 37 to 42% B over 25 min was used, with typical elution of 1CW between 38–39% B and that of 1CW-PEG750, 1CW-PEG2K, and 1CW-PEG5K between 40–41% B. For purification of H10H24, typical elution was ~42% B on a gradient from 41 to 45% B over 20 min. H10H24-PEG2K and H10H24-PEG5K eluted at ~39% B on a 30 to 40% B gradient over 30 min. Peptide elution was monitored with a diode array detector at wavelengths of 220 and 280 nm. The flow rate was 10 mL/min for semipreparative runs and peptides were injected at a concentration of 10–20 mg/mL.

MALDI-TOF Mass Spectrometry

The identity and purity of the peptides were verified by matrix-assisted laser desorption-ionization time-of-flight (MALDI-TOF) mass spectrometry using -cyano-4-hydroxycinnamic acid matrix. Mass spectra were recorded on an Applied BioSystems Voyager-DE Pro.

UV-Vis

Peptides were dissolved in buffered aqueous solution containing 25 mM potassium phosphate (KH_2PO_4) at pH 8 and 100 mM potassium chloride (KCl). Spectra were recorded on a Hewlett-Packard 8453 spectrophotometer using a standard 1 cm path length quartz cuvette. Peptide concentrations in solution were determined by their absorption at 280 nm due to each peptide's lone tryptophan residue, assuming an extinction coefficient of 5500 $\text{M}^{-1} \text{cm}^{-1}$, and using the Beer-Lambert Law.

Titration experiments were done using UV-vis spectroscopy with various concentrations of H10H24, H10H24-PEG2K, and H10H24-PEG5K solutions in quartz cuvettes. Spectra were recorded after addition of each aliquot, either 0.5 or 1 μL , depending on the concentration of hemin solution in DMSO, typically 200–500 μM , and the concentration of the peptide solution. The dissociation constant, K_d , of each heme binding site was determined by monitoring the shift of the heme absorbance at 412 nm as a function of the ratio of heme to four-helix bundles and assuming extinction coefficients of 120000 $\text{M}^{-1} \text{cm}^{-1}$ for bound heme and 35000 $\text{M}^{-1} \text{cm}^{-1}$ for free heme.²² K_d was calculated as $K_d = [A][B]/[AB]$, where

[A] is the concentration of free peptide in solution, [B] is the concentration of free heme in solution, and [AB] is the concentration of heme bound to H10H24. This specific titration experiment was repeated four times to ensure reproducibility. Detailed descriptions of the evaluation of the heme dissociation constants can be found in the Supporting Information.

Circular Dichroism

Circular dichroism measurements for secondary structure characterization were made on a Jasco J810 spectropolarimeter. CD spectra of each sample were recorded three times and averaged by collecting data from 260 to 190 at 0.2 nm intervals, a rate of 20 nm/min, a response time of 4 s, and a bandwidth of 1 nm. Samples were dissolved in 25 mM KH₂PO₄, 100 mM KCl buffer of various pH (3, 5, 8, 11). 1 mm path length quartz cuvettes were used for peptide concentrations > 10 µM, and 2 cm cuvettes were used for concentrations < 10 µM. Ellipticity was reported as the mean residue ellipticity ([], deg cm² dmol⁻¹) and calculated as [] = [_{obs} / (10dcn)], where [_{obs} is the measured ellipticity in millidegrees, d is the optical path length in cm, c is the concentration of the sample in mol/L, and n is the number of amino acids. The mean residue ellipticity for a 100% helix peptide of infinite length was taken to be -37400 deg cm² dmol⁻¹.³⁵ Temperature melt measurements were made of ~30 µM solutions of peptides dissolved in pH 8 potassium phosphate buffer in 1 mm path length quartz cuvettes. The ellipticity was monitored at 222 nm as the temperature increased from 5 to 95 °C in 5° increments, with a 1 min equilibration time at each temperature before the measurement was taken.

Analytical Ultracentrifugation

Sedimentation equilibrium experiments were performed on a Beckman Optima XL-A at 25 °C with samples solubilized in 25 mM KH₂PO₄, 100 mM KCl buffer at pH 8. The path length of the cells was 1.2 cm and the An-60Ti rotor was used. Measurements at 20000, 30000, and 40000 rpm were taken after 9 and 10 h of spinning at each speed to ensure equilibrium, which was verified by matching the early and late data sets. The radial distribution of absorbance was monitored at 280 nm. Sample concentrations were ~30, 60, and 120 µM, and sample volumes were 120 µL. To prevent the formation of disulfide bonds that result in the dimerization of 1CW in pH 8 buffer, 100 mM of *tris*(2-carboxyethyl)phosphine (TCEP) was added to the peptide solution. The specific volume of 1CW was calculated to be 0.7496 mL/g using the software Sednterp (<http://www.jphilo.mailway.com>) and those of 1CW-PEG2K and 1CW-PEG5K were calculated to be 0.7785 and 0.7972 mL/g, respectively, by a weighted average of specific volumes between the peptide and PEG (0.833 mL/g). Similarly, the specific volumes of H10H24 and H10H24-PEG2K were calculated to be 0.7627 and 0.7827 mL/g, respectively. The density of the buffer was 1.004 g/mL. Nonlinear global fits were made using the software program Heteroanalysis (<http://www.biotech.uconn.edu>).

Results and Discussion

Peptides that form coiled-coils are typically amphipathic helices with a hydrophobic patch along the length of the helix that drives the formation of helix bundles. By design, the interior of the helix bundle can be engineered to obtain specific binding affinities to various natural and unnatural prosthetic groups or to form channels of different shapes and sizes.^{23,36,37} While the interior of the helix bundle performs sophisticated reactions through specific recognition and binding, the exterior of the helix bundle influences the interaction with the environment.^{22,38–40} De novo protein design has shown that the exterior of the helix bundle can be tailored with specific patterns of charge or hydrophobicity so as to facilitate insertion into vesicles, orientation at interfaces, or assembly on solid substrates, while preserving the interior of the helix bundle, that is, its designed functionality.^{37,41–44}

Inspired by the findings of de novo protein design, it is possible to construct peptide–polymer conjugates by covalently linking polymer chains to the helix bundle-forming peptides without interfering with the interior of the helix bundles or sacrificing the designed functionalities. Peptide–polymer conjugates, using PEGylated coiled-coil helix bundle-forming peptides, were recently reported.^{7,14,20,45} The water-soluble conjugates were constructed by covalently linking PEG to the peptide N-terminus, forming essentially linear block copolymers. The presence of PEG was shown to enhance the stability of the peptide secondary structure against temperature and pH, acting as a shield between the peptide and its external environment. In the case of highly helix, long peptides, 35 and 42 amino acids in length, respectively, attaching a PEG chain to the N terminus did not affect the helix content nor interfere with homodimer formation.²⁰ However, for a shorter de novo designed coiled coil peptide, 23 amino acids in length, this architecture markedly decreased the helix content at peptide concentrations higher than 20 μM and lowered the degree of association.^{14,45}

It is possible that the attachment of PEG to the N-termini of the helix bundle restricts the volume available to the polymer chains, leading to molecular crowding and, thus, favoring lower aggregation states, as well as the unwinding of the ends of the helices, as depicted in Figure 1a. This effect becomes more obvious as the peptide's oligomeric state and the polymer molecular weight increase and the peptide length decreases. Examination of the molecular models of helix bundles suggest that PEG attachment to the sides of the bundle, rather than to an end, as shown schematically in Figure 1b, would lead to less steric occlusion. In this way, the peptide secondary structure and also tertiary structure would be retained. Additionally, attaching the polymer chains to the side of the helix bundle would allow both the peptide termini and the interior channel of the bundle to be more accessible.

Kochendoerfer et al. have synthesized a polymer-modified Erythropoiesis protein by covalently linking two branched polymers to a 166 amino-acid polypeptide chain.¹³ The polymer-modified Erythropoiesis protein formed a four-helix bundle with the branched polymers attached to the exterior of the bundle. It displayed full biological potency and increased in vivo lifetimes. In this case, four individual peptide segments were covalently linked together, and two branched polymers were conjugated to two of the four helices. It was not immediately clear how the branched polymers in this geometry affected the peptide secondary and tertiary structures.

Here, we present a new design of helix bundle-forming peptide–polymer conjugates by covalently linking a polymer chain to the peptide side chain. Figure 1b shows the helix wheel of a typical de novo designed three-helix bundle. The peptide primary structure is characterized by a heptad periodicity, -*abcdefg*-. Helix bundle formation is driven by the hydrophobic interactions between amino acids at positions *a* and *d* of each helix, forming a hydrophobic core. The bundle is further stabilized by the salt bridges between amino acids at positions *e* and *g* of adjacent helices.²³ We chose the polymer conjugation site to be the amino acid at position *f* in the middle of the peptide sequence, as shown schematically in Figure 1c, to minimize any potential interference with helix bundle stability.

Two families of peptide–PEG conjugates have been synthesized based on previously de novo designed coiled-coil helix bundle-forming peptides. The first peptide, 1CW, is based on a known peptide sequence, 28 amino acids in length, called “1coi” in the protein data bank.³³ The design of 1coi is very similar to the peptide sequences previously used to construct diblock copolymer type peptide–PEG conjugates.^{7,14,20,45} 1coi forms a coiled-coil three-helix bundle that is stabilized by nonpolar valines and leucines at positions *a* and *d*, respectively, and Glu-Lys salt bridges at positions *e* and *g*, respectively. Gly-Trp-Asp-Gly-Arg (GWDGR) was added to the N-terminus of 1coi for future study. Serine at position 16 (*f* position on the helix wheel) was mutated to cysteine to facilitate conjugation of maleimide

end-functionalized PEG. The second peptide studied, known as H10H24, is based on the diheme Cytochrome *b* subunit of cytochrome bc1.^{22,34} To conjugate end-functionalized PEG, the lysine at position 15 (*f* position on the helix wheel) was mutated to cysteine.³ PEG chains of three molecular weights, 750, 2000, and 5000 Da, were used to construct the peptide–PEG conjugates.

Peptide–PEG conjugates were purified by RP-HPLC and their identities and purities were verified by MALDI-TOF mass spectrometry. Figure 2 shows the mass spectrum of 1CW–PEG2K. The distance between two neighboring peaks is 44.05 Da, which is the mass of an ethylene glycol repeat unit. The lone peptides are perfectly monodispersed, so only the chain length heterogeneity of PEG contributes to the molecular weight distribution of the conjugate. In the MALDI-TOF mass spectrum, a representative peak is labeled with its mass, which corresponds to the sum of the masses of an integer number (42) of ethylene glycol units and the mass of the peptide segment. This confirms the chemical integrity of the conjugates. The mass spectra of the other peptide–polymer conjugates of varying PEG molecular weights can be found in the Supporting Information.

Characterizing the effects of the conjugated polymer chains on the structure and functionality of the helix bundle is key in defining the utility of the peptide–polymer conjugate assemblies. The secondary structures of the peptide and the peptide–PEG conjugates were investigated by circular dichroism (CD). Figure 3 shows the CD spectra of 30 μM solutions of 1CW, 1CW–PEG750, 1CW–PEG2K, and 1CW–PEG5K in potassium phosphate buffer at pH 8. All traces show typical α -helix characteristics, with minima at 222 and 208 nm and a maximum around 195 nm, as depicted in Figure 3. This data is evidence that PEG conjugation, for all molecular weights studied, enhances the helix content of the peptide. In addition, peptide helicity increases with an increase in PEG molecular weight: from ~63–66% for 1CW to ~72% for 1CW–PEG750 and ~80–83% for 1CW–PEG2K and 1CW–PEG5K. In the case of linear diblock copolymer type peptide–PEG conjugates, for relatively short sequences (23 amino acids), the presence of PEG-promoted helix formation only at low concentrations (<20 μM) and, subsequently, reduced the helix content at higher concentrations.¹⁴ PEG chains of larger molecular weight displayed a greater decrease in peptide helicity. For relatively longer peptides (33 and 42 amino acids), the conjugated PEG did not affect the helix content.^{14,20,45} In this study, conjugating PEG to the exterior of the helix bundle (33 amino acids) does indeed stabilize the secondary structure for all peptide concentrations studied, ~2–200 μM, and higher molecular weight PEGs, up to 5000 Da, do not unwind the helices.

Furthermore, the secondary structure of the conjugates at different pH values was investigated. The concentration dependence of the percent helicity of 1CW and 1CW–PEG2K in pH 3, 5, 8, and 11 buffers is plotted in Figure 4. For all pH values, peptide helicity increases with increased peptide concentration. At pH 3 and 5, the peptide exhibits high helix content, ~81%, at peptide concentrations above 20 μM, for both cases with and without conjugated PEG. At higher pH values (pH 8 and 11), the helicities of both the peptide and the conjugate decrease. However, the conjugates consistently display higher helix contents in comparison to their peptide counterparts. Conjugating PEG has the similar effect on helicity as reducing the pH. To exemplify, 1CW–PEG2K at pH 8 has a helix content near that of 1CW at pH 5. The common beliefs of the origin of enhanced helicity are that (1) PEG provides a microhydrophobic environment and (2) the presence of PEG introduces osmotic pressure that stabilizes the peptide/protein structure. Previous studies by H. Strey et al. have clearly shown that, using PEG as an osmolyte, osmotic pressure can be used to induce a random coil-to-helix transition in poly(glutamic acid) and has a similar effect to that of reducing the pH.^{46–48} In this case, the experimental results show similar effects, although PEG is now covalently linked to the peptide. Because we do not know the

spatial arrangement of the conjugated PEG chains relative to the peptide, the exact origin of the enhanced percent helicity is not immediately clear. In particular, the superposition between the effect of conjugated PEG and that of the pH is unknown.

The change in thermal stability of the peptide secondary structure upon PEG conjugation was investigated by taking temperature dependent CD measurements. Figure 5 shows the percent helicity as a function of temperature for 1CW, 1CW-PEG750, 1CW-PEG2K, and 1CW-PEG5K. Similar to what was seen at room temperature, the conjugated PEG stabilizes the peptide helices. The peptide-PEG conjugates display significantly higher helix contents than the peptide itself at all temperatures below 80 °C. At temperatures below 60 °C, 1CW-PEG5K displays a higher percent helicity than 1CW-PEG2K. This may be due to the greater presence of structured water molecules associated with the higher molecular weight PEG.^{47,48} There, however, does not appear to be a difference in the melting temperatures of the conjugates in relation to the peptide itself. All samples have a melting temperature in the range of 70–80 °C.

The effect of the conjugated PEG chains on helix bundle formation was determined using analytical ultracentrifugation (AUC). Figure 6 shows the sedimentation equilibrium analysis for 1CW, 1CW-PEG2K, and 1CW-PEG5K in pH 8 buffer. The self-organization of 1CW was best fit as an ideal species, yielding a fitted molecular weight of 10177 Da and an oligomeric state of 3. 1CW-PEG2K and 1CW-PEG5K were best fit as ideal species, yielding fitted molecular weights of 17147 and 25069 Da, respectively. These molecular weights also correspond to oligomeric states of 3. For all peptide concentrations investigated (30, 60, and 120 μM), 1CW-PEG2K and 1CW-PEG5K exhibit no distribution of monomers, dimers, or larger aggregates. Thus, the presence of PEG clearly does not interfere with the intended three-helix bundle formation.

Although CD spectra and AUC data both indicate that PEG does not deteriorate the peptide secondary or tertiary structures in this new design, it is unclear whether PEG may locally deform the peptide near the conjugation site and destroy an existing binding pocket in the interior of the bundle, which is essential for its designed functionality. To address this concern, cofactor binding can be used to assess the integrity of the helix bundle, especially for the purpose of generating functional biomolecular materials using peptide-polymer conjugates.

The second peptide studied, known as H10H24, is based on the diheme Cytochrome *b* subunit of cytochrome bc1.^{22,34} H10H24 contains two histidine binding sites at positions 10 and 24 and forms a coiled-coil four-helix bundle that can bind up to four hemes per bundle via bis-histidyl ligation. Each PEG chain is conjugated to cysteine at position 15 (*f* position on the helix wheel).³ H10H24 itself already displays a high helix content of ~81%. Upon conjugating PEG2K, only minimal changes in the helix content were observed (from ~81% for H10H24 to ~82% for H10H24-PEG2K). This is similar to the results of the diblock copolymer-type peptide-PEG conjugates with longer peptide sequences.^{20,45} Figure 7 shows the sedimentation equilibrium analysis of H10H24 and H10H24-PEG2K. For H10H24, the best fit of AUC data yielded a molecular weight of 12642 Da, which corresponds to an apparent oligomeric state of 3.4 instead of the intended four-helix bundle. This nonintegral degree of association has been observed previously;²² it was attributed to deviations in the partial specific volume of the protein complex from ideality because the sedimentation curves were independent of concentration over a wide range, and cross-linking the chains with disulfide bonds failed to change the apparent degree of association.²² Similarly, in the case of H10H24-PEG2K, the best fit yielded a molecular weight of 19260 Da and an oligomeric state of 3.36. Nonetheless, from the following heme-binding studies, we were

able to conclude that the conjugated PEG does not interfere with helix bundle formation nor disrupts the cofactor binding sites.

The effect of PEG conjugation on the interior of the helix bundle was investigated by studying heme titrations of H10H24, H10H24–PEG2K, and H10H24–PEG5K. Figure 8 shows the UV–vis spectra of the titration of a 200 μ M solution of heme in DMSO into an aqueous solution of 4 μ M H10H24–PEG2K. Agitation results in facile incorporation of heme into the peptides, as evidenced by an increase in the Soret peak at 412 nm and poorly resolved Q_1 and Q_2 bands at 560 and 529 nm, respectively. As more heme was added, the blue-shift in the peak, due to the absorbance of free heme in solution, was observed. Figure 8 inset plots the absorbance at 412 nm as a function of the heme to helix bundle ratio for H10H24–PEG2K. The change in slope of data sets for conjugated and nonconjugated peptides occurs at the same stoichiometry of heme to four-helix bundle, indicating that there is no substantial deleterious consequence of PEG conjugation. The heme titration experiments for H10H24–PEG5K also showed similar results. Multicofactor binding is a complicated phenomenon to quantify, so explicit determination of K_{d1} , K_{d2} , K_{d3} , and K_{d4} was not possible. Based on this data coupled with previous studies, H10H24–PEG2K, similar to H10H24, shows K_{d1} to be less than 1 nM and K_{d2} to be in the range of tens of nM, both of which are not measurable at this peptide concentration.^{22,31} We suspect no significant change in the first and second binding sites upon PEG conjugation and possibly slight interference with the third and fourth binding sites, based on the heme titration data fitting. Details on titration data fitting can be found in the Supporting Information. Nonetheless, K_{d3} for H10H24 and H10H24–PEG2K were both in the μ M range. Figure 9 compares the overlay of the UV–vis spectra of H10H24, H10H24–PEG2K, and H10H24–PEG5K upon additions of heme yielding heme: bundle ratios of 1:1, 2:1, 3:1, and 4:1. The UV–vis spectra of the *holo*- forms of H10H24–PEG2K and H10H24–PEG5K are essentially identical to that of H10H24, indicating that conjugated PEG does not interfere with the hydrophobic environment of heme, thus allowing retention of the designed functionality.

Conclusion

In summary, a new family of coiled-coil helix-forming peptide–polymer conjugates has been constructed by covalently linking PEG to the exterior of the helix bundle. Two types of de novo designed coiled-coil helix bundles were investigated, and it was shown that conjugated PEG chains promoted helix folding and retained coiled-coil associations. In this way, self-assembly of the peptides was greatly enhanced, and thermal stability was retained. In the case of a photoactive heme-binding peptide, PEG maintained the integrity of the binding sites and did not interfere with cofactor binding within the interior of the helix bundle.

This new peptide–polymer conjugate design strategy could be extended to other coiled-coil peptides. With this architecture, the peptide terminus is accessible and the peptide can be modified via various chemical motifs with tailored spatial arrangements and aggregation states. This allows the use of the important properties of coiled-coil helix bundle-based hydrogels for tissue engineering. The accessibility of both of the peptide termini could also enable the anchoring of a peptide–polymer conjugate monolayer onto a substrate. Additionally, polymer chains conjugated to the exterior of the helix bundle could provide a handle to mediate interactions between the bundle and its external environment, and allow the helix bundle-based machinery to function in nonbiological environments. The polymer chain could also mediate the interhelix bundle interactions, lead to their macroscopic assemblage, and consequently, achieve macroscopic responses of the peptides’ built-in functionalities. In conjunction with recent advances in de novo protein design, the newly designed architecture of helix bundle-forming peptide–polymer conjugates presented here

clearly shows great promise as a new avenue for peptide-based biomolecular functional materials.

Supplementary Material

Refer to Web version on PubMed Central for supplementary material.

Acknowledgments

We thank the Molecular Foundry at Lawrence Berkeley National Laboratory and Carolyn Bertozzi, University of California, Berkeley, for providing facilities to synthesize peptides. Work at the Molecular Foundry was supported by the Office of Science, Office of Basic Energy Sciences, of the U.S. Department of Energy under Contract No. DE-AC02-05CH11231. We also thank R. Dyche Mullins, Department of Cellular and Molecular Pharmacology, University of California, San Francisco, School of Medicine, for providing access to AUC experiments, and Kenneth Raymond, Department of Chemistry, and Susan Marqusee, Department of Molecular Cell Biology, University of California, Berkeley, for providing access to CD experiments. WFD thanks support from NIH Grant GM54616. The work was supported by the Laboratory Directed Research and Development Program at Lawrence Berkeley National Laboratory under Contract DE-AC02-05CH11232.

References and Notes

1. Duncan R. *Nat. Rev. Drug Discovery*. 2003; 2(5):347–360.
2. Harris JM, Chess RB. *Nat. Rev. Drug Discovery*. 2003; 2(3):214–221.
3. Kockendoerfer GG. *Curr. Opin. Chem. Biol.* 2005; 9:555–560. [PubMed: 16233987]
4. Borner HG, Schlaad H. *Soft Matter*. 2007; 3(4):394–408.
5. Klok HA, Vandermeulen GWM, Nuhn H, Rosler A, Hamley IW, Castelletto V, Xu H, Sheiko SS. *Faraday Discuss.* 2005; 128:29–41. [PubMed: 15658765]
6. Deming TJ. *Adv. Mater.* 1997; 9(4):299.
7. Petka WA, Harden JL, McGrath KP, Wirtz D, Tirrell DA. *Science*. 1998; 281(5375):389–392. [PubMed: 9665877]
8. Wang C, Stewart RJ, Kopecek J. *Nature*. 1999; 397:417–420. [PubMed: 9989405]
9. Hartgerink JD, Beniash E, Stupp SI. *Science*. 2001; 294(5547):1684–1688. [PubMed: 11721046]
10. Klok, Ha; Vandermeulen, GWM.; Nuhn, H.; Rosler, A.; Hamley, IW.; Castelletto, V.; Xu, H.; Sheiko, SS. *Faraday Discuss.* 2005; 128:29–41. [PubMed: 15658765]
11. Nowak AP, Breedveld V, Pakstis L, Ozbas B, Pine DJ, Pochan D, Deming TJ. *Nature*. 2002; 417(6887):424–428. [PubMed: 12024209]
12. Sarikaya M, Tamerler C, Schwartz DT, Baneyx FO. *Annu. Rev. Mater. Res.* 2004; 34:373–408.
13. Kochendoerfer GG, Chen SY, Mao F, Cressman S, Traviglia S, Shao HY, Hunter CL, Low DW, Cagle EN, Carnevali M, Gueriguiian V, Keogh PJ, Porter H, Stratton SM, Wiedeke MC, Wilken J, Tang J, Levy JJ, Miranda LP, Crnogorac MM, Kalbag S, Botti P, Schindler-Horvat J, Savatski L, Adamson JW, Kung A, Kent SBH, Bradburne JA. *Science*. 2003; 299(5608):884–887. [PubMed: 12574628]
14. Vandermeulen GWM, Tziatzios C, Klok HA. *Macromolecules*. 2003; 36(11):4107–4114.
15. Vandermeulen GWM, Klok HA. *Macromol. Biosci.* 2004; 4(4):383–398. [PubMed: 15468229]
16. Couet J, Jeyaprakash JD, Samuel S, Kopyshev A, Santer S, Biesalski M. *Angew. Chem. Int. Ed.* 2005; 44(21):3297–3301.
17. ten Cate MGJ, Severin N, Borner HG. *Macromolecules*. 2006; 39(23):7831–7838.
18. Kiick KL. *Polym. Rev.* 2007; 47(1):1–7.
19. Rosler, a; Klok, HA.; Hamley, IW.; Castelletto, V.; Mykhaylyk, OO. *Biomacromolecules*. 2003; 4(4):859–863. [PubMed: 12857065]
20. Pechar M, Kopeckova P, Joss L, Kopecek J. *Macromol. Biosci.* 2002; 2(5):199–206.
21. Akerfeldt KS, Lear JD, Wasserman ZR, Chung LA, Degrado WF. *Acc. Chem. Res.* 1993; 26(4): 191–197.

22. Robertson DE, Farid RS, Moser CC, Urbauer JL, Mulholland SE, Pidikiti R, Lear JD, Wand AJ, DeGrado WF, Dutton PL. *Nature*. 1994; 368(6470):425–431. [PubMed: 8133888]
23. DeGrado WF, Summa CM, Pavone V, Nastri F, Lombardi A. *Annu. Rev. Biochem.* 1999; 68:779–819. [PubMed: 10872466]
24. Micklatcher C, Chmielewski J. *Curr. Opin. Chem. Biol.* 1999; 3(6):724–729. [PubMed: 10600720]
25. Whaley SR, English DS, Hu EL, Barbara PF, Belcher AM. *Nature*. 2000; 405(6787):665–668. [PubMed: 10864319]
26. Moffet DA, Hecht MH. *Chem. Rev.* 2001; 101(10):3191–3203. [PubMed: 11710068]
27. Sakiyama-Elbert SE, Hubbell JA. *Annu. Rev. Mater. Res.* 2001; 31:183–201.
28. Cochran FV, Wu SP, Wang W, Nanda V, Saven JG, Therien MJ, DeGrado WF. *J. Am. Chem. Soc.* 2005; 127(5):1346–1347. [PubMed: 15686346]
29. Xu T, Wu SP, Miloradovic I, Therien MJ, Blasie JK. *Nano Lett.* 2006; 6(11):2387–2394. [PubMed: 17090063]
30. Razeghifard R, Wallace BB, Pace RJ, Wydrzynski T. *Curr. Protein Pept. Sci.* 2007; 8(1):3–18. [PubMed: 17305556]
31. Gibney BR, Johansson JS, Rabanal F, Skalicky JJ, Wand AJ, Dutton PL. *Biochemistry*. 1997; 36(10):2798–2806. [PubMed: 9062107]
32. Hawker CJ, Russell TP. *MRS Bull.* 2005; 30(12):952–966.
33. Ogihara NL, Weiss MS, Degrado WF, Eisenberg D. *Protein Sci.* 1997; 6(1):80–88. [PubMed: 9007979]
34. Huang SS, Gibney BR, Stayrook SE, Dutton PL, Lewis M. *J. Mol. Biol.* 2003; 326(4):1219–1225. [PubMed: 12589764]
35. Su JY, Hodges RS, Kay CM. *Biochemistry*. 1994; 33(51):15501–15510. [PubMed: 7803412]
36. Discher BM, Lear JD, Moser CC, Dutton PL. *Biophys. J.* 2002; 82(1):458A–458A. [PubMed: 11751332]
37. Hecht MH, Das a, Go A, Bradley LH, Wei YN. *Protein Sci.* 2004; 13(7):1711–1723. [PubMed: 15215517]
38. Discher BM, Koder RL, Moser CC, Dutton PL. *Curr. Opin. Chem. Biol.* 2003; 7(6):741–748. [PubMed: 14644184]
39. Ye SX, Discher BM, Strzalka J, Xu T, Wu SP, Noy D, Kuzmenko I, Gog T, Therien MJ, Dutton PL, Blasie JK. *Nano Lett.* 2005; 5(9):1658–1667. [PubMed: 16159202]
40. Ye SX, Strzalka JW, Discher BM, Noy D, Zheng SY, Dutton PL, Blasie JK. *Langmuir*. 2004; 20(14):5897–5904. [PubMed: 16459607]
41. Discher BM, Noy D, Strzalka J, Ye SX, Moser CC, Lear JD, Blasie JK, Dutton PL. *Biochemistry*. 2005; 44(37):12329–12343. [PubMed: 16156646]
42. Churbanova IY, Tronin A, Strzalka J, Gog T, Kuzmenko I, Johansson JS, Blasie JK. *Biophys. J.* 2006; 90(9):3255–3266. [PubMed: 16473900]
43. Pilloud DL, Chen XX, Dutton PL, Moser CC. *J. Phys. Chem. B.* 2000; 104(13):2868–2877.
44. Chen XX, Discher BM, Pilloud DL, Gibney BR, Moser CC, Dutton PL. *J. Phys. Chem. B.* 2002; 106(3):617–624.
45. Vandermeulen GWM, Tziatzios C, Duncan R, Klok HA. *Macromolecules*. 2005; 38(3):761–769.
46. Strey HH, Parsegian VA, Podgornik R. *Phys. Rev. Lett.* 1997; 78(5):895–898.
47. Parsegian, Va; Rand, RP.; Fuller, NL.; Rau, DC. *Methods Enzymol.* 1986; 127:400–416. [PubMed: 3736427]
48. Stanley CB, Strey HH. *Biophys. J.* 2002; 82(1):458A–458A. [PubMed: 11751332]

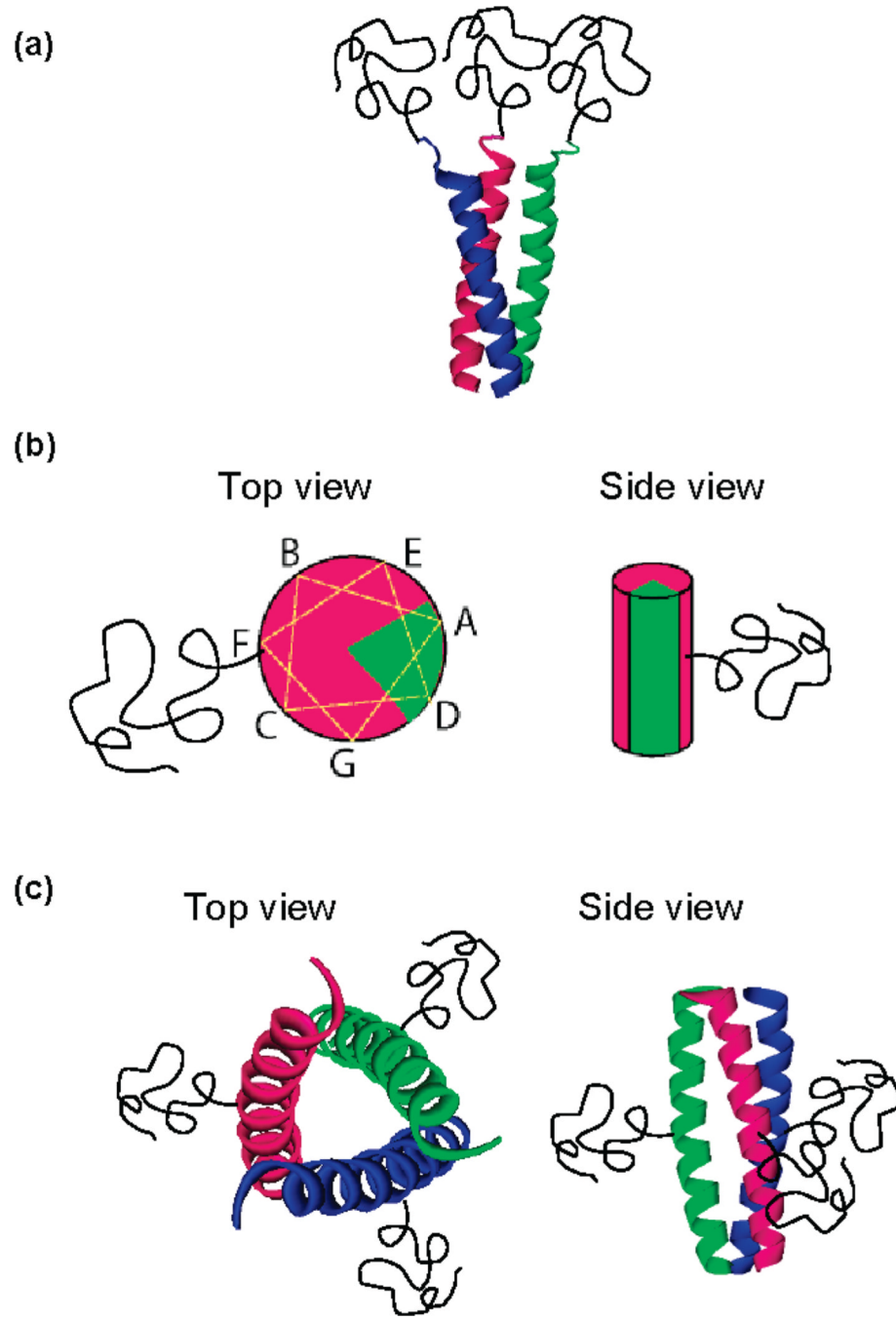


Figure 1.

Schematic drawings of two designs of helix bundle peptide–polymer conjugates using a coiled-coil three-helix bundle-forming peptide as an example: (a) polymers are conjugated to the end of the helix bundle, potentially creating steric hindrance and disrupting helix bundle formation; this effect becomes more obvious as the peptide’s oligomeric state and the polymer molecular weight increase and the peptide length decreases; (b) top view, depicting the helix wheel, and side-view of the new design of peptide–polymer conjugates, with the polymer attached to the side chain of the amino acid in the middle of the peptide sequence; (c) schematic drawing of the new peptide–polymer conjugate design, with polymer chains conjugated to the exterior of the helix bundle, potentially stabilizing helix bundle formation.

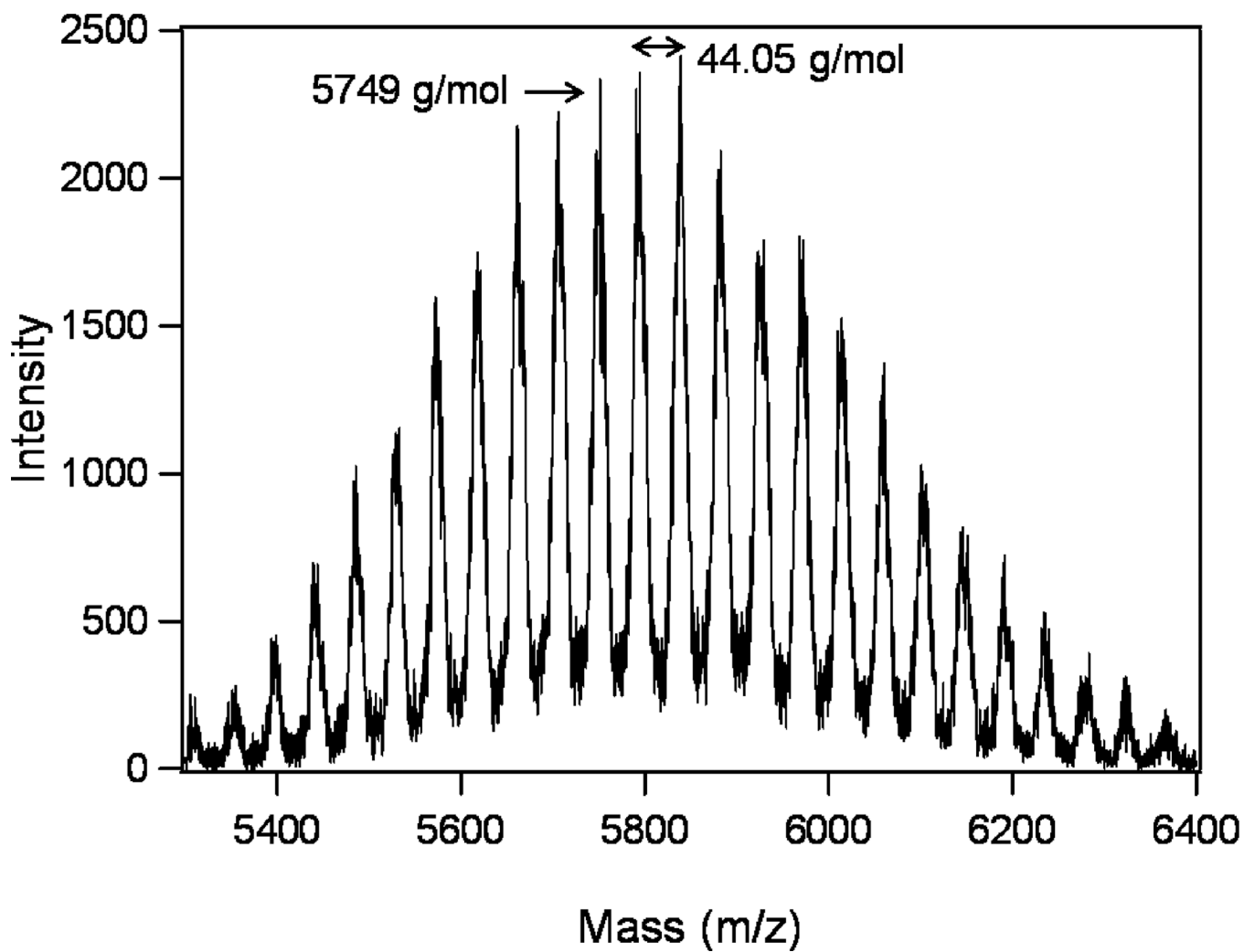


Figure 2.

MALDI-TOF mass spectrum of 1CW-PEG2K. The distance between two neighboring peaks is 44.05 Da, the mass of an ethylene glycol repeat unit. The labeled peak corresponds to the sum of the masses of an integer number (42) of ethylene glycol units and the mass of the monodisperse peptide segment.

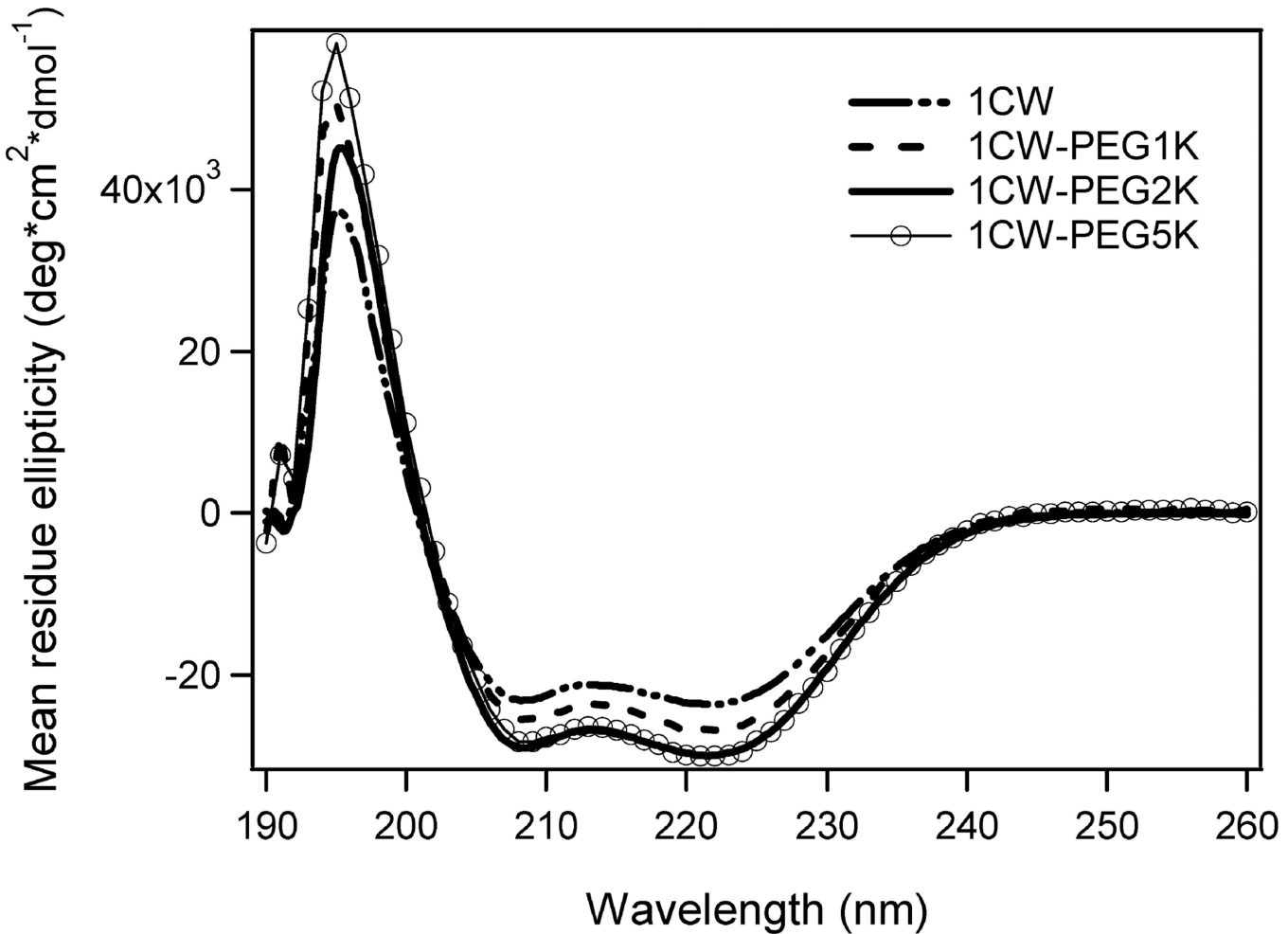


Figure 3.

CD spectra of 30 μM solutions of 1CW, 1CW-PEG750, 1CW-PEG2K, and 1CW-PEG5K in 25 mM KH_2PO_4 buffer at pH 8 and 25 $^{\circ}\text{C}$. All traces exhibit typical α -helix characteristics.

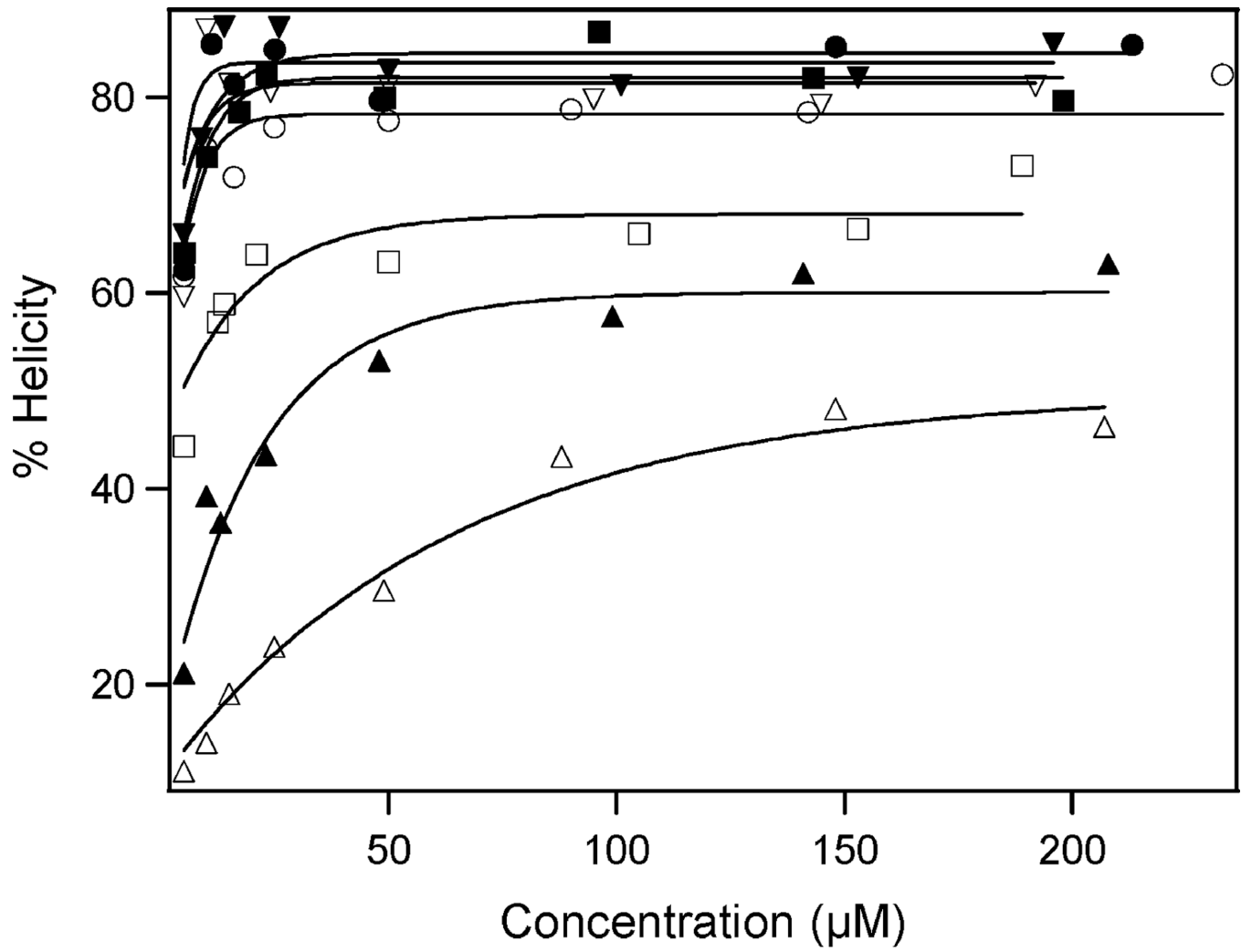


Figure 4.

Concentration dependence of percent helicity of 1CW and 1CW-PEG2K in pH 3, 5, 8, and 11 buffers at 25 °C. The solid markers represent 1CW-PEG2K at the following pH: () pH 3, () pH 5, () pH 8, and () pH 11. The corresponding unfilled markers represent 1CW at each respective pH.

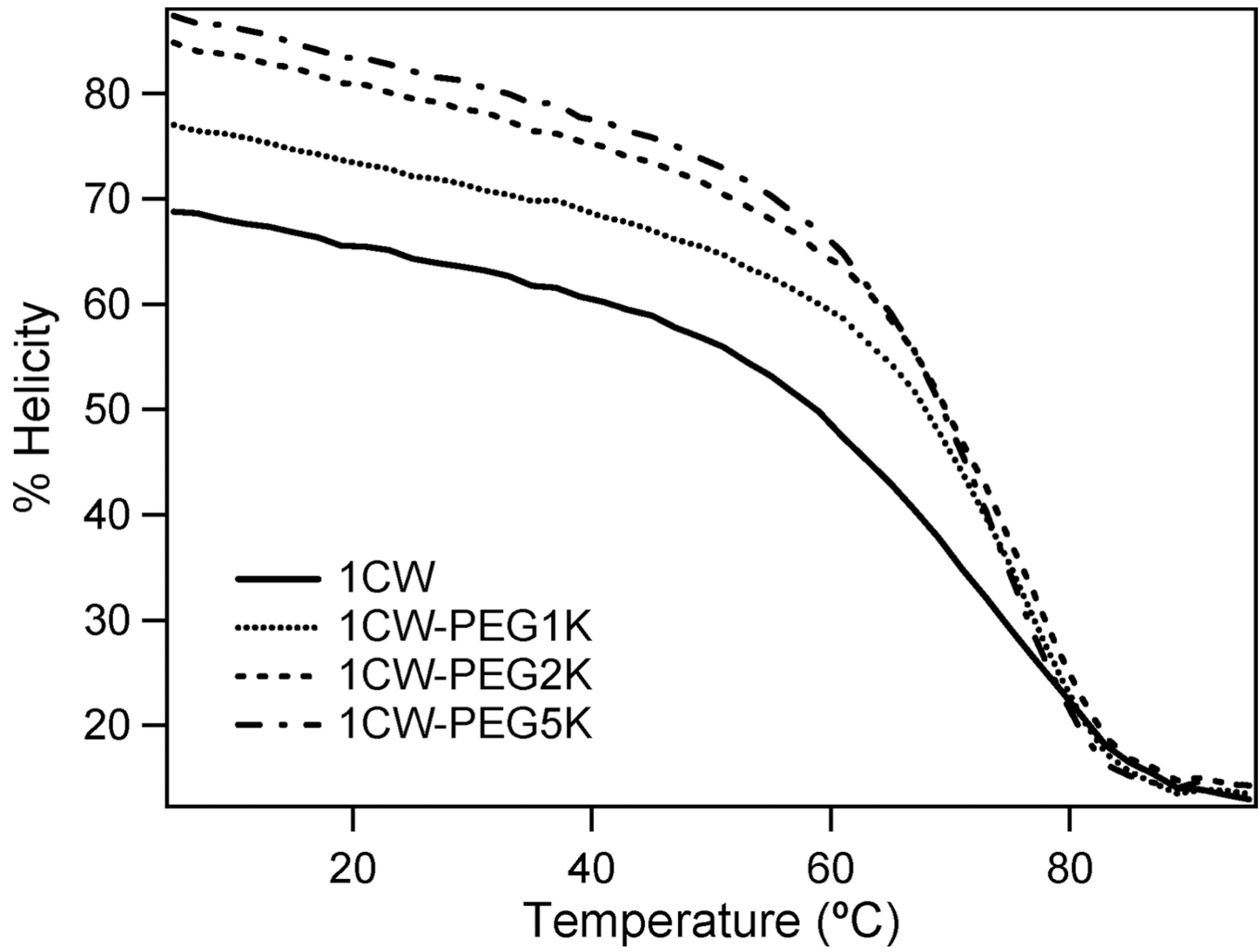


Figure 5.

CD temperature melts of 30 μM solutions of 1CW, 1CW-PEG750, 1CW-PEG2K, and 1CW-PEG5K in pH 8 buffer.

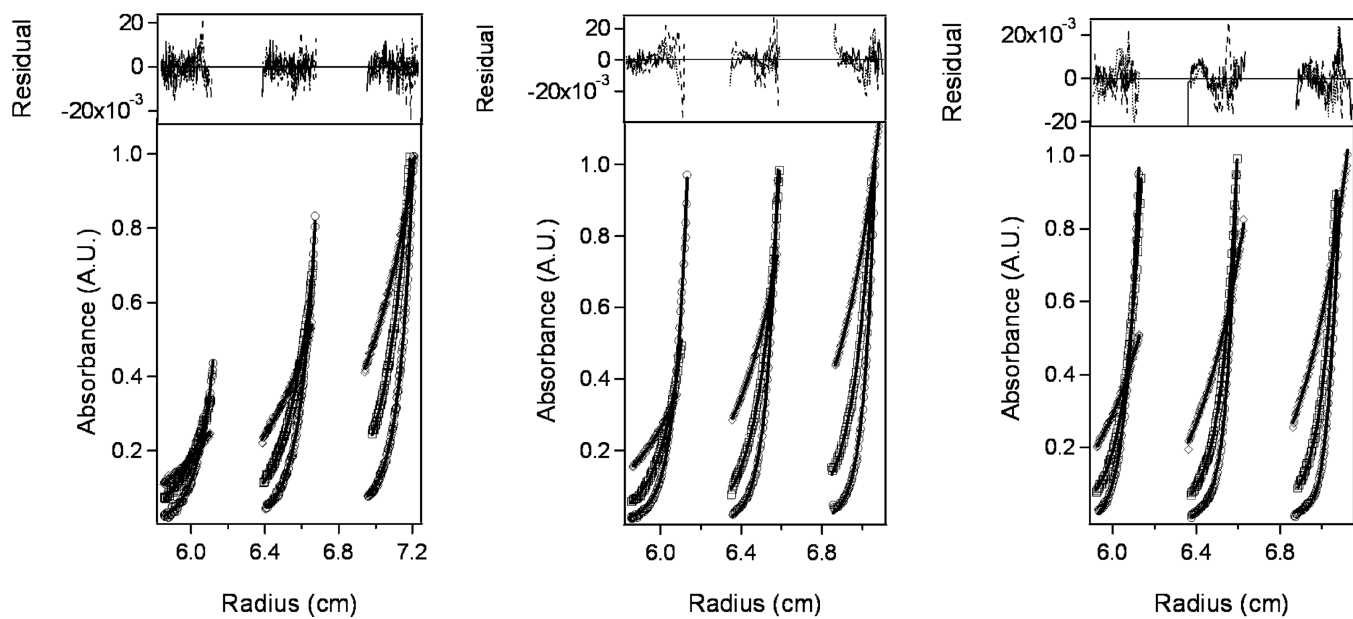


Figure 6.

AUC sedimentation equilibrium radial absorbance profiles of 30, 60, and 120 μM solutions of (left) 1CW, (middle) 1CW-PEG2K, and (right) 1CW-PEG5K at speeds of 20K, 30K, and 40K rpm. Raw data are shown as symbols and their global fits as solid lines. The residuals for each fit appear above the radial absorbance profiles. The fitting of 1CW and its conjugates agree with single ideal species of three-helix bundles.

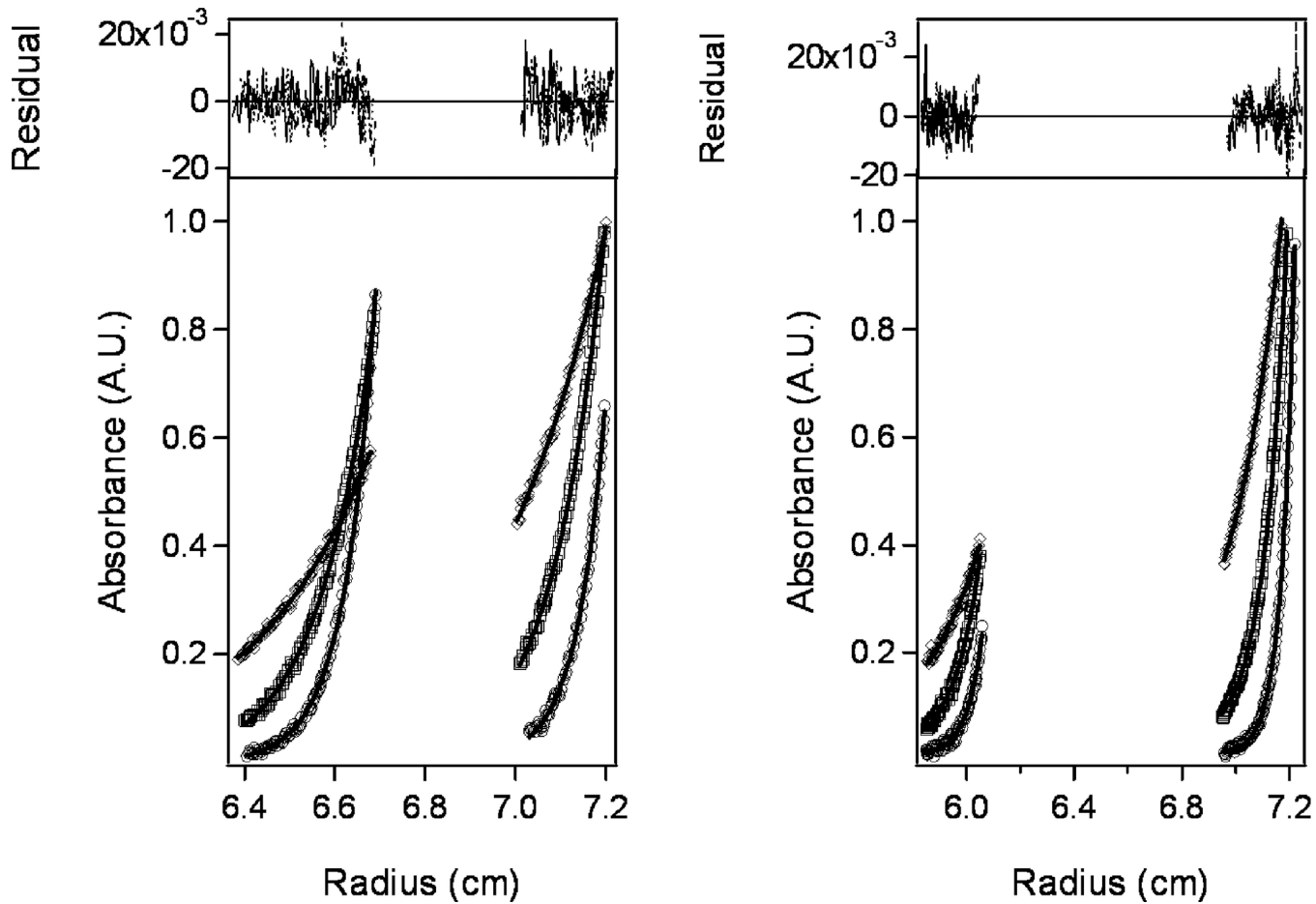
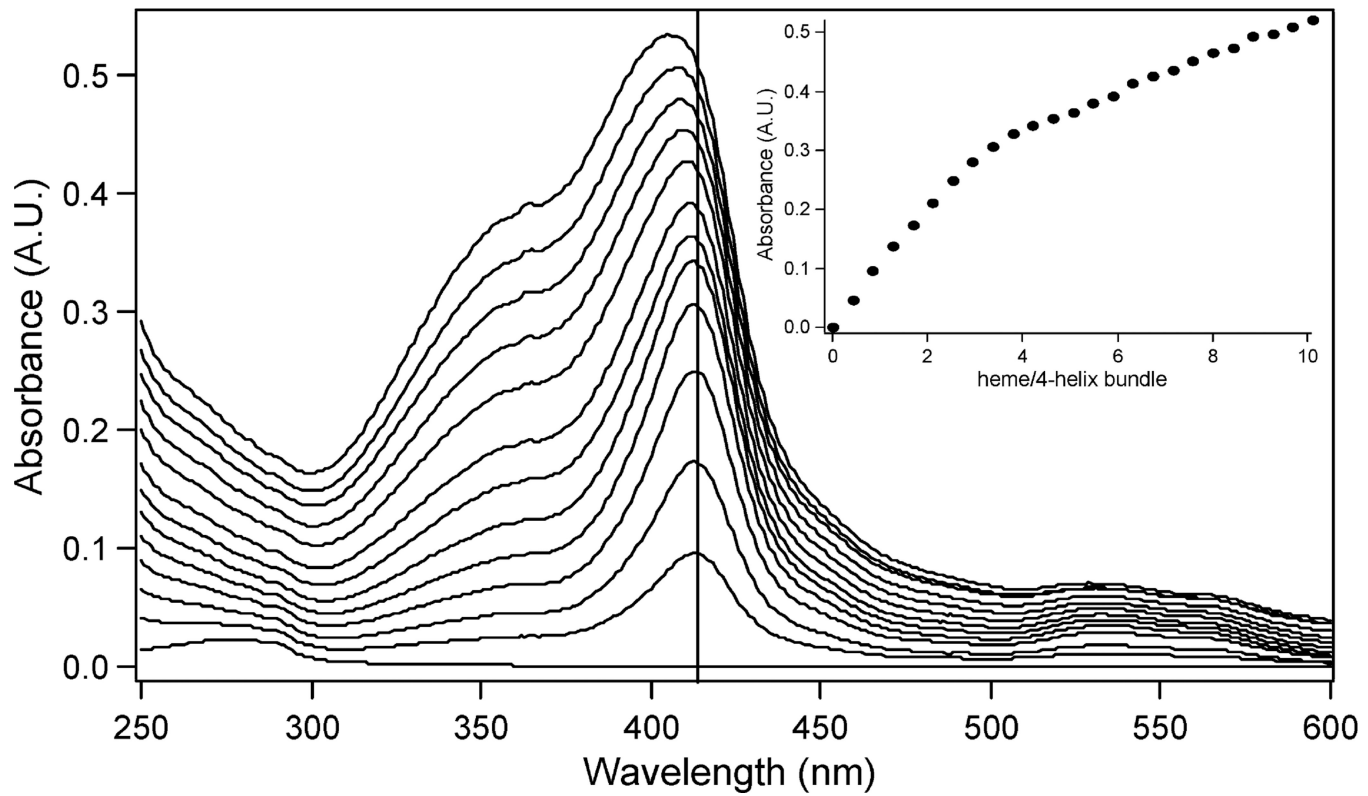


Figure 7.

AUC sedimentation equilibrium radial absorbance profiles of 30, 60, and 120 μM solutions of (left) H10H24 and (right) H10H24–PEG2K at speeds of 20K, 30K, and 40K rpm. Raw data are shown as symbols and their global fits as solid lines. The residuals for each fit appear above the radial absorbance profiles. The nonintegral fitting of H10H24 and its conjugates agree with previous work,²² indicating the presence of four-helix bundles.

**Figure 8.**

(a) UV-vis spectra of heme titrations into a 4 μ M solution of H10H24-PEG2K recorded in a 1 cm path length cuvette, upon addition of 0, 0.8, 1.7, 2.5, 3.3, 4.1, 5.0, 5.8, 6.6, 7.5, 8.3, 9.1, and 10.0 equiv of heme per four-helix bundle. A vertical line indicates the peak at 412 nm. The dissociation constants were determined from the absorbance at 412 nm vs the [heme]/[four-helix bundle] ratio, as shown in the inset.

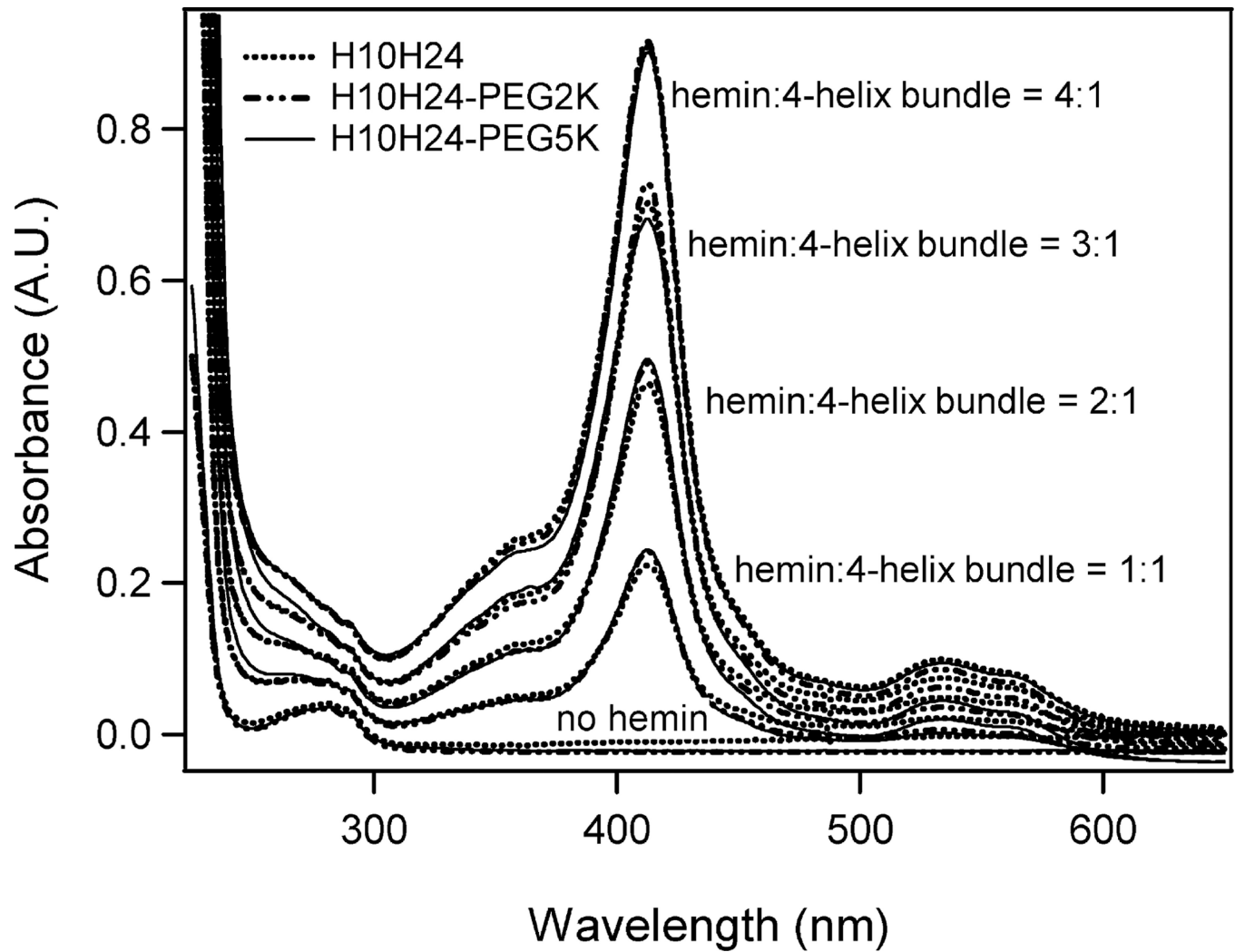


Figure 9.

UV-vis spectra of heme titrations into 10 μ M solutions of H10H24, H10H24-PEG2K, and H10H24-PEG5K recorded in a 1 cm path length cuvette, upon addition of 0, 1, 2, 3, and 4 equiv of heme per four-helix bundle.